Article:
Guo, C. Y., Zhang, W. Q., Huang, H. et al. (37 more authors) (2024) Spectroscopy of 187Tl: shape coexistence. European Physical Journal A : Hadrons and Nuclei. 165. ISSN 1434-601X

https://doi.org/10.1140/epja/s10050-024-01395-3

Spectroscopy of ^{187}Tl: Shape coexistence

C. Y. Guo,[1] W. Q. Zhang,[2,3] H. Huang,[2,3] S. Q. Zhang,[1] Z. H. Li,[1,*] Z. Liu,[2,3,†] H. Hua,[1] D. W. Luo,[1] H. Y. Wu,[4,1] A. N. Andreyev,[5,6] D. Seweryniak,[7] B. Andel,[8,9] S. Antalic,[8] A. E. Barzakh,[10] M. Block,[11,12,13] A. Bronis,[8] M. P. Carpenter,[7] P. Copp,[7] J. G. Cubiss,[5] D. T. Doherty,[14] P. Van Duppen,[9] Z. Favier,[15] F. Giacoppo,[11,12] B. Kindler,[12] F. G. Kondev,[7] T. Lauritsen,[7] X. Q. Li,[1] B. Lommel,[12] M. Al Monthery,[5] P. Mošať,[8] L. Ni,[1] C. Raison,[5] W. Reviol,[7] G. Savard,[7] S. Stolze,[7] G. L. Wilson,[16] C. Xu,[1] J. Z. Zhang,[1] S. Y. Zhang,[1] and Z. X. Zhou[1]

[1]*School of Physics and State Key Laboratory of Nuclear Physics and Technology, Peking University, Beijing 100871, China*
[2]*Institute of Modern Physics, Chinese Academy of Sciences, Lanzhou 730000, China*
[3]*University of Chinese Academy of Sciences, Beijing 100049, China*
[4]*Key Laboratory of Nuclear Data, China Institute of Atomic Energy, Beijing 102413, China*
[5]*School of Physics, Engineering and Technology, University of York, York, YO10 5DD, United Kingdom*
[6]*Advanced Science Research Center (ASRC), Japan Atomic Energy Agency, Tokai-mura, Japan*
[7]*Physics Division, Argonne National Laboratory, Argonne, IL60439, USA*
[8]*Department of Nuclear Physics and Biophysics, Comenius University in Bratislava, 84248 Bratislava, Slovakia*
[9]*KU Leuven, Instituut voor Kern-en Stralingsfysica, 3001 Leuven, Belgium*
[10]*Petersburg Nuclear Physics Institute, NRC Kurchatov Institute, 188300 Gatchina, Russia*
[11]*Helmholtz-Institut Mainz, Mainz, 55128, Germany*
[12]*GSI Helmholtzzentrum für Schwerionenforschung Darmstadt, Darmstadt, 64291, Germany*
[13]*Johannes-Gutenberg Universität, Mainz, 55099, Germany*
[14]*Department of Physics, University of Surrey, Guildford, GU2 7XH, United Kingdom*
[15]*Physics Department, CERN, 1211 Geneva 23, Switzerland*
[16]*Department of Physics and Astronomy, Louisiana State University, Baton Rouge, LA 70803, USA*

(Dated: February 13, 2024)

The prompt and delayed γ-ray spectroscopy of ^{187}Tl was studied via the ^{142}Nd(^{50}Cr, $3p2n$)^{187}Tl fusion-evaporation reaction at a beam energy of 255 MeV. An enhanced level scheme of ^{187}Tl was established. The collective bands with one-quasiparticle configurations from the $2f_{7/2}$, $1h_{9/2}$, $1h_{11/2}$ and $1i_{13/2}$ orbitals and high-lying structures with possible three-quasiparticle configurations are investigated in terms of the tilted axis cranking covariant density functional theory. At low excitation energy, the rotational bands with one-quasiparticle configurations reflect the shape coexistence of three shapes: prolate, triaxial, and oblate. The possible shapes of two microsecond isomers at high excitation energy are proposed.

I. INTRODUCTION

The nuclear shape that reflects the spatial distribution of the nucleons is a fundamental characteristic of the nucleus. The possible shapes which the nucleus adopts result from the competition and delicate balance between the collective and single-particle degrees of freedom. Therefore, nuclear shape provides a sensitive probe of the underlying nuclear structure and a stringent test for nuclear structure models. In the region around $Z = 82$ and $A = 180$, there are large shell gaps at both prolate and oblate deformation around the neutron mid-shell at $N = 104$–106. The nuclei in this region exhibit rich shape-related phenomena, particularly the shape coexistence, and have long been the active topic of research [1]. For example, the shape coexistence manifests itself in ^{186}Pb through the occurrence of three low-lying 0^+ states with prolate, oblate, and spherical shapes, respectively [2].

Due to the different polarization effects of the different single-particle orbitals on the nuclear shapes, the spectroscopy of odd-A nuclei can provide important clues for understanding the mechanism behind the shape coexistence, and therefore attracts particular interest. Studies of odd-A nuclei in this region have revealed the coexistence of distinct shapes not only at low excitaions but also at high-lying isomeric states [1].

In this paper, we report the in-beam and delayed γ-ray spectroscopy of ^{187}Tl. For the light thallium isotopes ($Z = 81$), the collective structures have revealed the coexistence of different nuclear shapes [1], where the important deformation driving orbitals are the $\pi h_{9/2}$ and $\pi i_{13/2}$ intruders. Previously, the nucleus ^{187}Tl has been studied via decay spectroscopy [3–6], in-beam γ-ray spectroscopy [7–10], and laser spectroscopy [11–13]. Four prolate bands and two oblate bands were established [8]. Meanwhile, two isomers with microsecond lifetimes ($T_{1/2} = 1.11$ μs and 0.69 μs) were also observed [6], but their shapes and configurations were uncertain. In the present study, with high selectivity of the prompt and delayed γ-ray spectroscopy, a more complete level scheme of ^{187}Tl has been established, with which the shape co-

* zhli@pku.edu.cn
† liuzhong@impcas.ac.cn

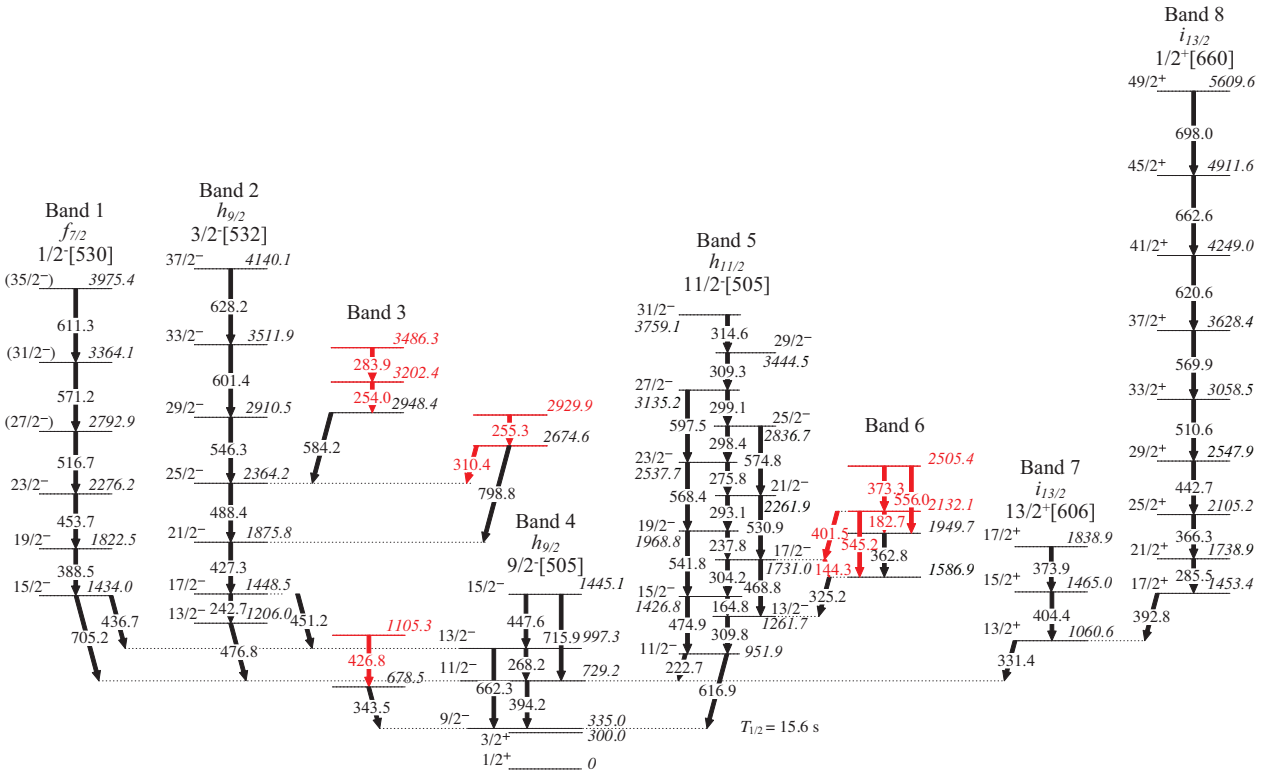

FIG. 1. Partial level scheme of ^{187}Tl deduced from prompt γ rays. The excitation energies of the $3/2^+$ state at 300.0 keV and the $9/2^-$ state at 335.0 keV are taken from Refs. [6, 8, 10]. Energies are in keV. New transitions and levels are marked as red.

existence within a wide excitation energy range in ^{187}Tl is discussed.

II. EXPERIMENTAL SETUP

The present experiment was performed at the ATLAS superconducting linear accelerator, at Argonne National Laboratory (ANL). The ^{187}Tl nuclei were produced via the ^{142}Nd(^{50}Cr, $3p2n$)^{187}Tl fusion-evaporation reaction at beam energy of 255 MeV with an average intensity of 7 pnA. Targets with a thickness of $\approx$ 700 $\mu g/cm^2$ (including fluorine) were prepared from $^{142}NdF_3$ material with an isotopic enrichment of $\approx$ 99.8%. Four target sectors were mounted on a rotating wheel, and the beam was wobbled to $\pm$2.5 mm horizontally across the target by a magnetic steerer to avoid the target melting.

Prompt γ rays at the target position were detected by the Gammasphere array with 64 large-volume Compton-suppressed Ge detectors at the time of the experiment. The typical energy resolution and detection efficiency for Gammasphere were $\approx$ 3.5 keV (FWHM) and $\approx$ 12% for γ-ray energies around 300 keV. Evaporation residues (EVRs) were separated from the primary beam by the Argonne Gas-Filled Analyzer (AGFA) filled with $\approx$ 0.65 mbar helium gas and transported to the focal-plane detector system. The typical time of flight (ToF) of recoils through AGFA is around 500 ns. A position sensitive parallel grid avalanche counter (PGAC), located at the exit from AGFA, provided time of arrival and energy-loss signals of EVRs. The recoiling nuclei were subsequently implanted into a 300 μm thick, 64 mm $\times$ 64 mm double-sided silicon strip detector (DSSD with 160×160 strips) located 40 cm behind the PGAC. The coincidence between signals from the PGAC and the DSSD enabled implantation of ions to be distinguished from decays. Gamma rays emitted from the EVRs and their daughters were detected by four HPGe clover detectors (X-array) surrounding the DSSD [14]. The typical energy resolution and detection efficiency for the X-Array were $\approx$ 3.4 keV (FWHM) and $\approx$ 16% for γ-ray energies around 250 keV. The data for ^{187}Pb, ^{183}Hg, ^{188}Bi, and ^{188}Po from the same experiment were previously presented in Refs. [15–17]

III. DATA ANALYSIS AND RESULTS

A. Prompt γ Rays of ^{187}Tl

Approximately 1.2×10^8 prompt γ-γ coincident events were collected in the Gammasphere, from which a symmetric matrix was built. The level scheme analysis was performed using the RADWARE software [18]. To de-

termine the multipolarities of the γ-ray transitions, two asymmetric angular distributions from oriented states (ADO) matrices were constructed by using the γ rays detected at all angles (the y axis) against those detected at 50°+130° and 80°+100° (the x axis), respectively. The multipolarities of the emitted γ rays were analyzed by means of the ADO ratio, defined as $(I_\gamma(\ 50°) + I_\gamma(\ 130°))/(I_\gamma(\ 80°) + I_\gamma(\ 100°))$. In general, the typical ADO ratios for the stretched quadrupole and stretched pure dipole transitions are found to be ≈ 0.9 and ≈ 0.7, respectively.

The collective structures of ^{187}Tl have been previously studied by many experiments, for example employing ^{159}Tb(^{32}S, $4n$)^{187}Tl [8–10] and ^{156}Gd(^{35}Cl, $4n$)^{187}Tl [7] fusion-evaporation reactions. Rotational bands built upon the $1/2^-[530]$ of $2f_{7/2}$, $3/2^-[532]$ and $9/2^-[505]$ of $1h_{9/2}$, $11/2^-[505]$ of $1h_{11/2}$, $1/2^+[660]$ and $13/2^+[606]$ of $1i_{13/2}$ proton orbitals with prolate or oblate shapes have been established. The present analyses confirm these levels and support the previous spin-parity assignments. The partial level scheme of ^{187}Tl deduced from the present prompt γ-ray spectra is shown in Fig. 1. It was constructed from the γ-γ coincidence relationships, intensity balances and ADO ratios. The results are summarized in Table I. The typical γ-ray spectra which support the proposed level scheme are shown in Fig. 2.

TABLE I: γ-ray energies, excitation energies, relative γ-ray intensities, ADO ratios and spin-parity assignments in ^{187}Tl.

E_γ (keV)	E_i (keV)	Relative Intensity	R_{ADO}	$I_i^\pi \rightarrow I_f^\pi$	Multipolarity
144.3(2)	1731.0(2)				
164.8(1)	1426.8(2)	5.2(3)	0.61(8)	$15/2^- \rightarrow 13/2^-$	M1
182.7(1)	2132.1(2)				
222.7(1)	951.9(1)	8.3(4)	0.82(10)	$11/2^- \rightarrow 11/2^-$	M1/E2
237.8(1)	1968.8(2)	5.9(4)		$19/2^- \rightarrow 17/2^-$	
242.7(1)	1448.5(2)	4.5(3)		$17/2^- \rightarrow 13/2^-$	
254.0(1)	3202.4(3)	3.4(3)			
255.3(1)	2929.9(3)	6.2(6)			
268.2(1)	997.3(1)	11.0(4)	0.87(9)	$13/2^- \rightarrow 11/2^-$	M1/E2
275.8(1)	2537.7(3)	3.4(4)		$23/2^- \rightarrow 21/2^-$	
283.9(2)	3486.3(4)				
285.5(1)	1738.9(2)	100.0	1.07(4)	$21/2^+ \rightarrow 17/2^+$	E2
293.1(2)	2261.9(3)	5.8(3)		$21/2^- \rightarrow 19/2^-$	
298.4(2)	2836.7(3)			$25/2^- \rightarrow 23/2^-$	
299.1(2)	3135.2(3)			$27/2^- \rightarrow 25/2^-$	
304.2(1)	1731.0(2)	11.6(8)	0.85(16)	$17/2^- \rightarrow 15/2^-$	M1/E2
309.3(2)	3444.5(4)			$29/2^- \rightarrow 27/2^-$	
309.8(1)	1261.7(2)	19.3(4)	1.00(12)	$13/2^- \rightarrow 11/2^-$	M1/E2
310.4(3)	2674.6(3)				
314.6(1)	3759.1(4)			$31/2^- \rightarrow 29/2^-$	
325.2(1)	1586.9(2)	8.1(6)			
331.4(1)	1060.6(1)	148.0(24)	0.89(4)	$13/2^+ \rightarrow 11/2^-$	E1/M2
343.5(1)	678.5(1)				
362.8(1)	1949.7(2)				
366.3(1)	2105.2(2)	81.2(38)	1.01(4)	$25/2^+ \rightarrow 21/2^+$	E2
373.3(1)	2505.4(3)				
373.9(1)	1838.9(2)	8.8(7)		$17/2^+ \rightarrow 15/2^+$	
388.5(1)	1822.5(2)	100.0[b]	0.97(9)	$19/2^- \rightarrow 15/2^-$	E2
392.8(1)	1453.4(2)	279.9(28)[a]		$17/2^+ \rightarrow 13/2^+$	
394.2(1)	729.2(1)			$11/2^- \rightarrow 9/2^-$	
401.5(1)	2132.1(2)				
404.4(1)	1465.0(2)	11.3(21)	0.60(6)	$15/2^+ \rightarrow 13/2^+$	M1
426.8(2)	1105.3(2)				
427.3(1)	1875.8(2)	60.3(8)	0.98(6)	$21/2^- \rightarrow 17/2^-$	E2
436.7(1)	1434.0(2)	8.4(7)		$15/2^- \rightarrow 13/2^-$	

TABLE I. (*Continued*).

442.7(1)	2547.9(2)	52.3(24)	1.19(5)	$29/2^+ \rightarrow 25/2^+$	E2
447.6(2)	1445.1(2)			$15/2^- \rightarrow 13/2^-$	
451.2(1)	1448.5(2)	64.0(17)	1.12(6)	$17/2^- \rightarrow 13/2^-$	E2
453.7(1)	2276.2(2)	78.7(38)[b]	1.25(10)	$23/2^- \rightarrow 19/2^-$	E2
468.8(1)	1731.0(2)	5.7(6)		$17/2^- \rightarrow 13/2^-$	
474.9(1)	1426.8(2)	13.5(7)	0.88(10)	$15/2^- \rightarrow 11/2^-$	E2
476.8(1)	1206.0(2)	12.0(9)		$13/2^- \rightarrow 11/2^-$	
488.4(1)	2364.2(2)	41.7(13)	1.18(7)	$25/2^- \rightarrow 21/2^-$	E2
510.6(1)	3058.5(3)	33.7(15)	0.85(4)	$33/2^+ \rightarrow 29/2^+$	E2
516.7(1)	2792.9(3)	41.0(27)[b]		$(27/2^-) \rightarrow 23/2^-$	
530.9(2)	2261.9(3)	5.4(3)		$21/2^- \rightarrow 17/2^-$	
541.8(2)	1968.8(2)			$19/2^- \rightarrow 15/2^-$	
545.2(1)	2132.1(2)				
546.3(1)	2910.5(3)	18.4(10)	0.92(10)	$29/2^- \rightarrow 25/2^-$	E2
556.0(3)	2505.4(3)				
568.4(2)	2537.7(3)			$23/2^- \rightarrow 19/2^-$	
569.9(1)	3628.4(3)	21.5(10)	1.00(4)	$37/2^+ \rightarrow 33/2^+$	E2
571.2(1)	3364.1(3)	32.3(23)[b]		$(31/2^-) \rightarrow (27/2^-)$	
574.8(1)	2836.7(3)	4.9(2)		$25/2^- \rightarrow 21/2^-$	
584.2(2)	2948.4(3)	5.3(4)			
597.5(2)	3135.2(3)			$27/2^- \rightarrow 23/2^-$	
601.4(2)	3511.9(3)	9.4(11)		$33/2^- \rightarrow 29/2^-$	
611.3(2)	3975.4(4)	20.6(18)[b]		$(35/2^-) \rightarrow (31/2^-)$	
616.9(1)	951.9(1)	36.2(27)	1.09(9)	$11/2^- \rightarrow 9/2^-$	M1/E2
620.6(1)	4249.0(3)	16.4(8)		$41/2^+ \rightarrow 37/2^+$	
628.2(2)	4140.1(4)	2.8(2)		$37/2^- \rightarrow 33/2^-$	
662.3(1)	997.3(1)	51.9(37)	0.98(5)	$13/2^- \rightarrow 9/2^-$	E2
662.6(1)	4911.6(4)	7.7(4)		$45/2^+ \rightarrow 41/2^+$	
698.0(2)	5609.6(4)			$49/2^+ \rightarrow 45/2^+$	
705.2(2)	1434.0(2)	5.6(4)		$15/2^- \rightarrow 11/2^-$	
715.9(2)	1445.1(2)	4.9(3)		$15/2^- \rightarrow 11/2^-$	
798.8(2)	2674.6(3)	6.4(4)			

[a] Total intensity of the 392.8- and 394.2-keV γ-rays.
[b] Since the energies of the low-lying γ-rays in band 1 are close to their neighboring stronger peaks, the intensities of transitions in band 1 are normalized to the intensity of 388.5-keV γ-rays.

The bands 1, 2, and 8 built on the $1/2^-[530]$ of $2f_{7/2}$, $3/2^-[532]$ of $1h_{9/2}$, and $1/2^+[660]$ of $1i_{13/2}$ orbitals, respectively, as well as the bands 4 and 7 built on the $9/2^-[505]$ of $1h_{9/2}$ and $13/2^+[606]$ of $1i_{13/2}$ orbitals, respectively, are observed up to the same levels as in Ref. [8]. In Ref. [8], a transition sequence of 309.8, 325.1, and 362.7 keV was assigned as an $11/2^-[505]$ band with a bandhead at 951.9 keV. In the follow-up work [10] with the same ^{159}Tb(^{32}S, $4n$)^{187}Tl fusion-evaporation reaction as that in Ref. [8], the $1h_{9/2}$ band (band 2 in the present work) extended from spin $37/2^-$ at 4.139 MeV to spin $45/2^-$ at 5.519 MeV. Meanwhile, a new rotational band built on the $11/2^-[505]$ of $1h_{11/2}$ orbital has been established, in which only the 309.8-keV transition was included [10]. Our work supports the level sequence of the $11/2^-[505]$ band reported in Ref. [10]. In addition, in the present work the 362.8-keV transition is assigned as the member of a new structure (band 6 in Fig. 1), and the 325.2-keV transition is assigned as an interband transition from the state at 1586.9 keV in band 6 to the $13/2^-$ state at 1261.7 keV in band 5. The band 3 is also newly established.

B. Delayed γ Rays of ^{187}Tl

As we mentioned above, two isomers with microsecond lifetimes ($T_{1/2}$ = 1.11 μs and 0.69 μs) in ^{187}Tl have been reported, although their spin-parities and decay paths were not firmly determined [6]. To further probe the

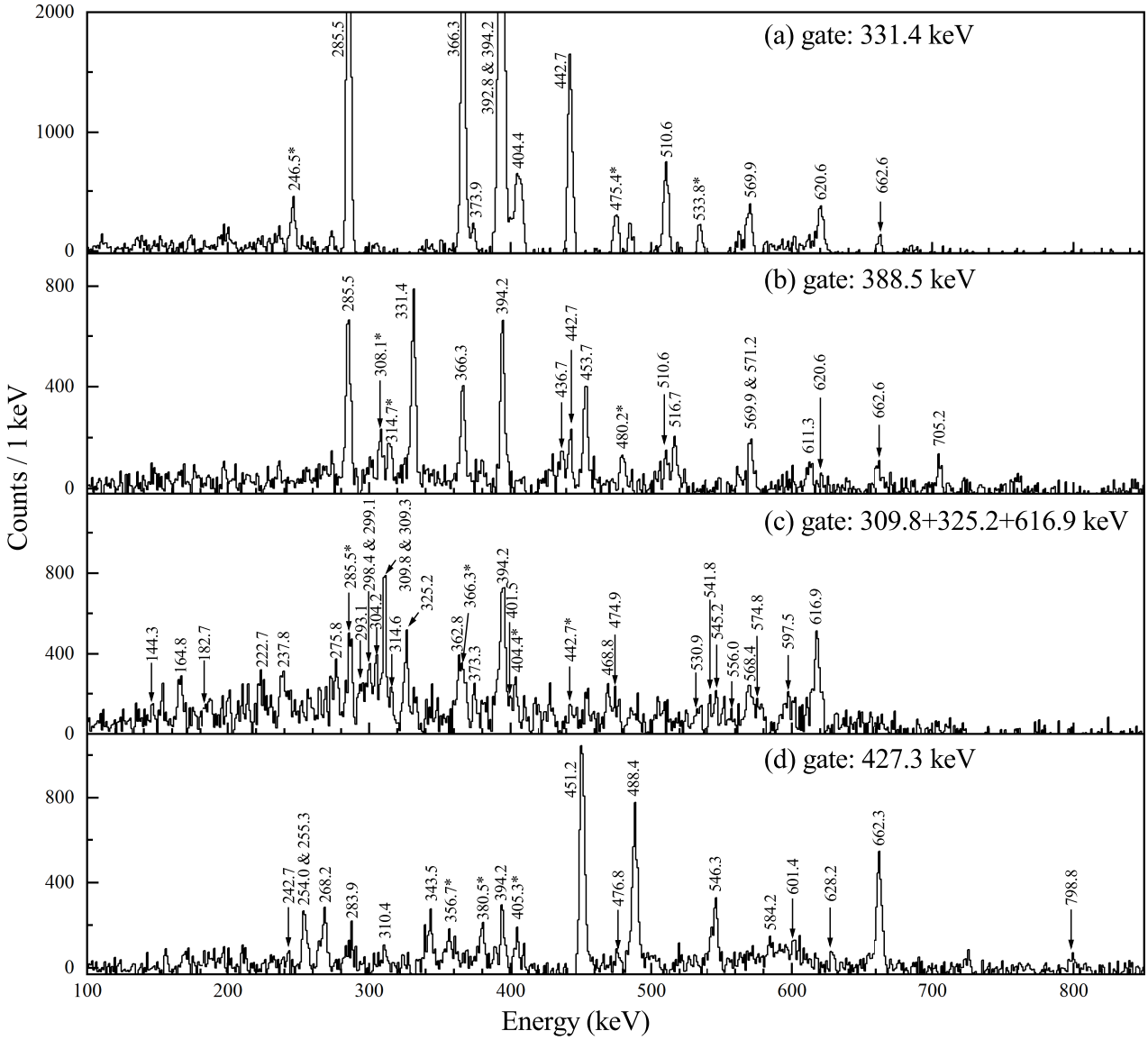

FIG. 2. Coincident prompt γ-ray spectra for ^{187}Tl, gated on the (a) 331.4 keV transition, (b) 388.5 keV transition, (c) 309.8 + 325.2 + 616.9 keV transitions, and (d) 427.3 keV transition. The peaks marked with stars ($*$) are known contaminants from other nuclei.

properties of these two isomers in ^{187}Tl, a symmetric matrix was built from the delayed γ rays measured by the X-array, with a time window of 0–3 μs after the implantation of EVRs into DSSD. The partial level scheme related to these two isomers is shown in Fig. 3 and the typical γ-ray spectra are shown in Fig. 4.

The present work supports the decay scheme of the isomer at 2.584 MeV reported in Ref. [6]. Spin-parities $J^\pi = 25/2^-, 27/2^\pm, 29/2^+$ were tentatively assigned to this isomer based on the deduced total conversion coefficient of 0.15(18) for the 479.4 keV line from a balance of intensities, which suggest multipolarities of $E1$, $M1$ or $E2$ [6]. In the present work, a total conversion coefficient of 0.17(10) is deduced and consistent with the previous value of 0.15(18).

In Ref. [6], the position of the $T_{1/2} = 1.11\ \mu s$ isomer was uncertain. A transition cascade of 191.0 and 201.6 keV decaying from this isomer was reported. This isomer was found to decay via two parallel paths to the low-lying states: one deexcites to the $13/2^-$ state at 1261.7 keV and the other to the $17/2^+$ state at 1453.4 keV [6]. Not all γ rays linking this isomer to low-lying states in ^{187}Tl were observed, thus the position of this isomer was not determined [6].

In the present work, as shown in delayed spectrum in Fig. 4(b), seven transitions of 164.8, 304.2, 325.2, 401.5, 468.8, 474.9, and 545.2 keV, are found to be in coincidence with the 616.9- and 309.8-keV transitions, suggesting that these seven transitions lie in the decay path to the $13/2^-$ state at 1261.7 keV. Therefore, four levels are

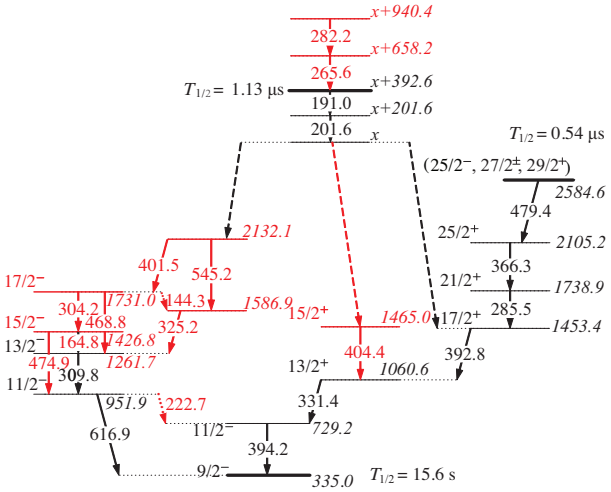

FIG. 3. Partial level scheme for ^{187}Tl, with decay paths for the two isomers and feeding path to the 1.1-μs isomer. The dashed lines show the existence of these decay paths, but their exact nature is not known. The 144.3- and 222.7-keV transitions shown in dotted lines are too weak to be clearly seen in the isomer decay. Energies are in keV. The transitions and levels observed for the first time in the isomer decays, as well as new transitions and levels above the isomer, are marked in red.

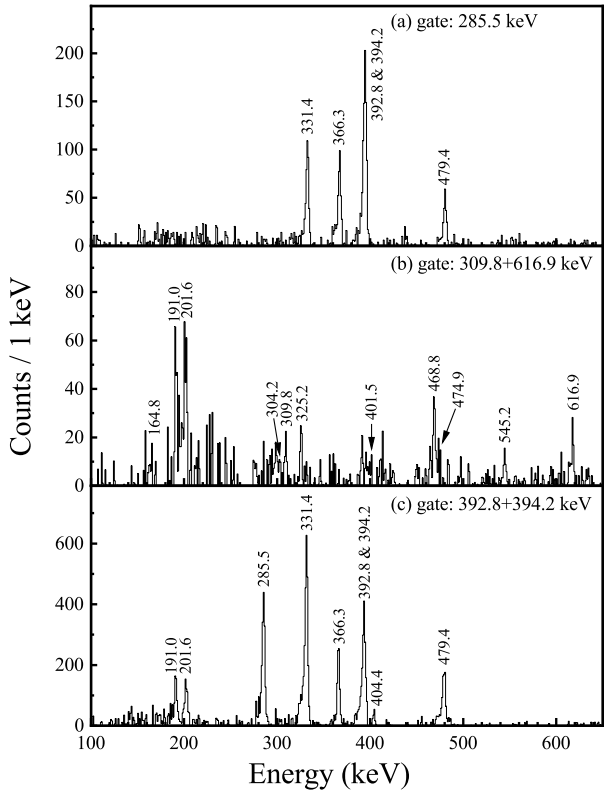

FIG. 4. Coincident delayed spectra for ^{187}Tl, gated on the (a) 285.5 keV transition, (b) 309.8 + 616.9 keV transitions, and (c) 392.8+394.2 keV transitions.

added to this path. In addition, as shown in Fig. 4(c), the 404.4-keV transition in band 7 is in coincidence with the 394.2-keV transition, which means there is another new decay path to the low-lying $13/2^+$ state at 1060.6 keV. Unfortunately, since there are still missing γ rays linking this isomer to low-lying states, its position can not be determined.

Gating on sum of the 191.0- and 201.6-keV transitions, the decay curve was constructed from the time difference between the implantation and subsequent γ rays and shown in Fig. 5(a), yielding a half-life of 1.13(10) μs, which is consistent with the reported value of 1.11(7) μs [6]. When gating on the 479.4-keV transition, the decay curve yields a half-life of 0.54(5) μs (see Fig. 5(b)) for the isomer at 2584.6 keV, which is smaller than the reported value of 0.69(4) μs in Ref. [6].

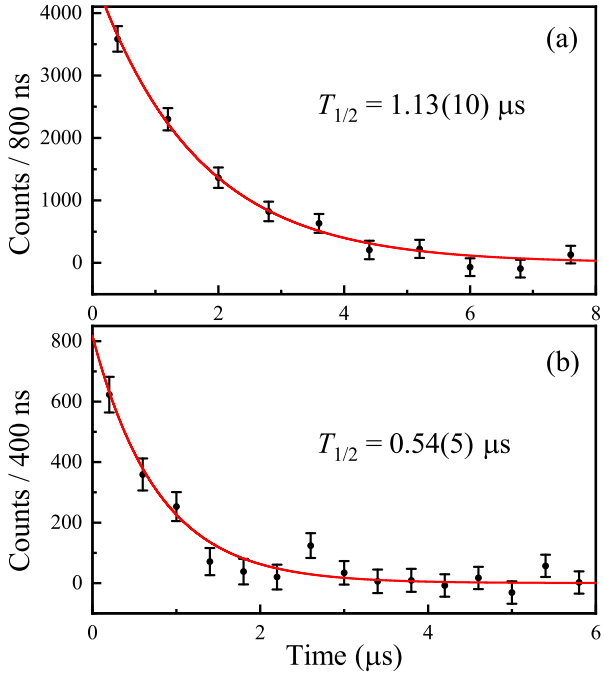

FIG. 5. The background subtracted time difference (ΔT(EVR-γ)) for the (a) 191.0 + 201.6 keV transitions and (b) 479.4 keV transition. A least-squares fit is performed for the exponential decay, and shown by the red line.

C. γ rays feeding the isomeric state of ^{187}Tl

To determine the transitions feeding the isomeric state, the isomer-decay tagging (IDT) method [19] was used and a prompt - delayed matrix was established. As shown in Fig. 6(a) and (b), when gating on the delayed 392.8-, 394.2- and 331.4-keV γ -rays, as well as the delayed 191.0-keV γ-ray, two new γ-rays of 265.6 and 282.2 keV can be clearly seen in the prompt spectra. To see the relationship between these two new γ-rays, another symmetric prompt γ-γ matrix was created, which only included

the γ-rays detected in Gammasphere array in coincidence with the delayed γ-rays of 392.8, 394.2 and 331.4 keV detected in X-array. As shown in the inset of Fig. 6(a), the 265.6-keV transition has a clear coincidence with the 282.2-keV transition. Therefore, based on the new observation of these two γ-rays, their coincidence relationship, and their intensities (I_γ(282.2 keV)/I_γ(265.6 keV) = 0.86), two new levels are added above the isomer with half-life of 1.13(10) μs.

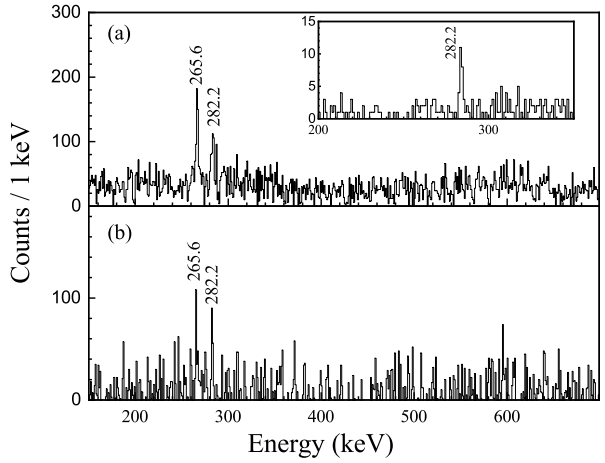

FIG. 6. Prompt spectra for ^{187}Tl, gated on the delayed (a) 331.4 + 392.8 + 394.2 keV transitions and (b) 191.0 keV transition. Inset: Prompt spectrum with gates on the prompt 265.6 keV transition and sum of the delayed 331.4 + 392.8 + 394.2 keV transitions.

IV. DISCUSSION

In previous studies [7–10], the low-lying collective structures observed in ^{187}Tl have revealed the coexistence of different nuclear shapes. Here, to obtain further insight into the rotational bands built on the single-particle orbitals close to the Fermi surface and their corresponding shapes in ^{187}Tl, the tilted axis cranking covariant density functional theory TAC-CDFT [20–22] calculations are performed. The relativistic point-coupling density functional PC-PK1 [23] with a basis of 12 major oscillator shells is adopted in the particle-hole channel, and the pairing correlations are neglected for simplicity.

In Fig. 7, the calculated energy spectra built upon the $2f_{7/2}$, $1h_{9/2}$, $1h_{11/2}$ and $1i_{13/2}$ orbitals are plotted as a function of the rotational frequency, and compared with the available data for bands 1, 2, 5 and 8, respectively. The agreements between theoretical and experimental data are good. At high rotational frequency (>300 keV), the deviations of the theoretical results from the experimental data become large, which can be ascribed to the alignment of a pair of $i_{13/2}$ neutrons in these bands [8, 10].

For the $\pi h_{9/2}$ configuration in band 2 (Fig. 7(b)), the TAC-CDFT calculation predicts a pair of $3d_{3/2}$ protons

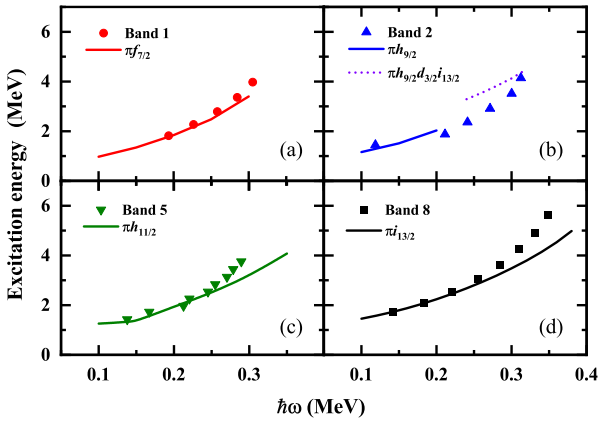

FIG. 7. The calculated energy spectra as functions of rotational frequency by TAC-CDFT calculations in comparison with the experimental data for (a) band 1, (b) band 2, (c) band 5, and (d) band 8 of ^{187}Tl.

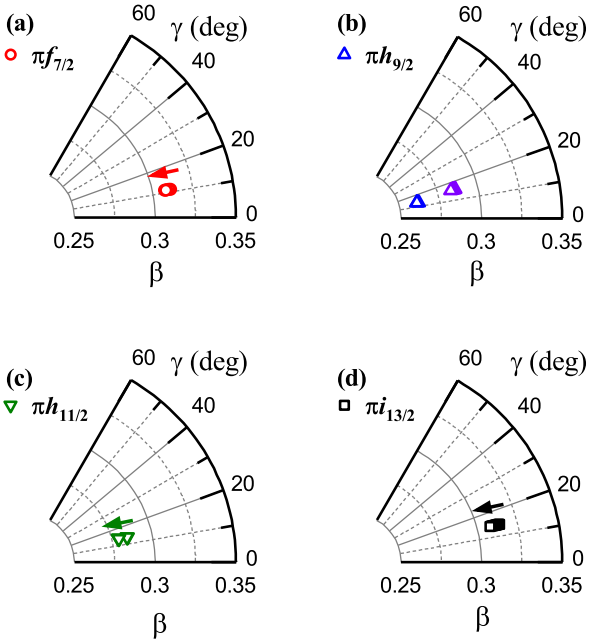

FIG. 8. The evolutions of deformation parameters β and γ driven by increasing rotational frequency in the TAC-CDFT calculations for (a) band 1, (b) band 2, (c) band 5, and (d) band 8 in ^{187}Tl. The arrows indicate the increasing direction of the rotational frequency $\hbar\omega$, which changes from 0.10 MeV to 0.30 MeV in all cases. Note the points with larger deformation in panel (b) correspond to the calculated results with a proton pair broken for $\hbar\omega > 0.22$ MeV.

broken around $\hbar\omega \approx 0.22$ MeV. These two unpaired protons occupy the $3d_{3/2}$ orbital and the $1i_{13/2}$ orbital, respectively. Above the rotational frequency 0.22 MeV, the calculated energy spectra deviate from the experimental energy spectra of band 2. The inclusion of pairing correlations may delay this breaking and give a better agreement with band 2.

TABLE II. Possible three-quasiparticle configurations for the isomeric states in ^{187}Tl. The excitation energy, deformation parameters β and γ are calculated by the TAC-CDFT with the density functional PC-PK1.

K^π	Shape	Quasiparticles	Configuration	Energy	β	γ
$25/2^+$	Prolate	1p2n	$\pi 11/2^-[505] \otimes \nu 9/2^+[624]5/2^-[512]$	1.396 MeV	0.283	11.0°
$27/2^-$	Prolate	1p2n	$\pi 11/2^-[505] \otimes \nu 9/2^+[624]7/2^+[633]$	1.876 MeV	0.279	14.8°
$23/2^+$	Oblate	1p2n	$\pi 9/2^-[505] \otimes \nu 9/2^+[624]5/2^-[532]$	0.526 MeV	0.177	60.0°
$23/2^-$	Oblate	1p2n	$\pi 13/2^+[606] \otimes \nu 7/2^+[613]3/2^-[501]$	3.800 MeV	0.186	60.0°
$27/2^-$	Oblate	1p2n	$\pi 13/2^+[606] \otimes \nu 9/2^+[624]5/2^-[532]$	3.311 MeV	0.179	60.0°
$27/2^+$	Oblate	3p	$\pi 13/2^+[606]9/2^-[505]5/2^-[503]$	4.946 MeV	0.236	60.0°
$29/2^+$	Oblate	3p	$\pi 13/2^+[606]9/2^-[505]7/2^-[514]$	3.480 MeV	0.236	60.0°

In previous works [7–10], bands 1, 2, 5 and 8 were suggested to have prolate shapes, while bands 4 and 7 were suggested to have oblate shape. Meanwhile, the triaxial degree of freedom was found to play a role in these collective structures [8, 10]. To examine the possible shape coexistence and the involved triaxiality, Fig. 8 shows the calculated deformation parameters β and γ for bands 1, 2, 5, and 8 in the TAC-CDFT, as well as the evolutions of their deformations with the rotational frequency. It can be seen that the calculated β values lie around 0.28 for bands 2 and 5, whereas the corresponding values are larger than 0.30 for bands 1 and 8. The deformation enhancement of the latter can be ascribed to the occupation of the high-j low-Ω deformation driving orbital, i.e., $1/2^-[530]$ of $\pi f_{7/2}$ for band 1 and $1/2^+[660]$ of $\pi i_{13/2}$ for band 8. The γ values for these bands are very similar, in the range of 12-15°. With the increase of the rotational frequency, the quadrupole deformation parameter β decreases smoothly while γ changes very slightly. Only for the $\pi h_{9/2}$ band, the unpairing of the $3d_{3/2}$ protons to the low-Ω $i_{13/2}$ orbital leads to a deformation increase around $\hbar\omega \approx 0.22$ MeV. The calculated β values are consistent with the previous calculations [7, 8]. In contrast to the triaxial prolate deformation of bands 1, 2, 5, and 8, bands 4 and 7 are found to have an axial symmetric oblate deformation with $\beta = 0.185$, $\gamma = 60°$ and $\beta = 0.190$, $\gamma = 60°$, respectively, and behave in a similar way.

It is worthwhile to investigate the nature of the two μs isomeric states. In Ref. [6], the 2584.6-keV isomer has assignments constrained to the range $J^\pi = 25/2^-$, $27/2^\pm$, or $29/2^+$, which suggests a high-K three-quasiparticle configuration. According to the decay scheme in Fig. 3, the other isomer with a half-life of 1.13 μs most probably has a comparable excitation energy and a similar range of J^π, indicating a high-K three-quasiparticle configuration, too. Moreover, the two isomeric states might have either a prolate-like triaxial or an oblate shape, as discussed for the one-quasiparticle bands. Since the spin-parity assignments for these two isomers are not determined, their configurations can only be discussed in a general manner. As a further reference, the TAC-CDFT calculations for several low-lying three-quasiparticle configurations have been performed at $\hbar\omega = 0$ MeV to obtain the deformation information at the corresponding bandheads. The results are given in Table II.

For prolate deformation, the low-lying three-quasiparticle configuration of ^{187}Tl with quantum number K no less than 25/2 should involve the $11/2^-[505]$ proton configuration. The two candidates listed in Table II couple this proton with the two-quasineutron excitation $\nu 9/2^+[624]7/2^+[633]$ and $\nu 9/2^+[624]5/2^-[512]$, respectively, which behave prolate-like triaxial in shape with $\beta_2 \approx 0.28$ and $\gamma \approx$ 10-15°. For oblate deformation, the one high-K quasiproton could either be $9/2^-[505]$ from the $h_{9/2}$ orbital or $13/2^+[606]$ from the $i_{13/2}$ orbital. This proton can couple either with two-quasineutron or two-quasiproton excitation to form a low-lying high-K three-quasiparticle configuration. As seen in Table II, there are several possibilities and the three-quasiproton configurations have a relatively larger oblate shape ($\beta \approx 0.24$) than the one-quasiproton-two-quasineutron ones ($\beta \approx 0.18$).

Considering that the 2584.6-keV isomer decays to band 8 with the $\pi 1/2^+[660]$ configuration and does not feed band 5 with the $\pi 11/2^-[505]$ configuration, this isomer is unlikely to be prolate-like with the quasiproton $11/2^-[505]$ configuration involved. Thus the 2584.6-keV isomer is more likely to be a high-K shape isomer with an oblate shape, decaying to a distinguished prolate-like shape. The other high-K isomer has comparative decay paths to the low-lying levels in three bands. It is more likely to be another shape isomer of a three-quasiproton configuration with both the $\pi 9/2^-[505]$ and $\pi 13/2^+[606]$ components involved.

V. SUMMARY

The spectroscopy of ^{187}Tl was studied via the ^{142}Nd(^{50}Cr, $3p2n$) fusion-evaporation reaction at a beam energy of 225 MeV. Eight collective structures built on one-quasiparticle configurations are investigated in terms

of the TAC-CDFT. The agreements between the experimental energy spectra and the calculations are good. The evolutions of the deformation parameters β and γ driven as a function of the rotational frequency in the TAC-CDFT calculations are presented. It is proposed that bands 1, 2, 5, and 8 have a prolate deformation with a 12-15° γ value, while the bands 4 and 7 are associated with an axial symmetric oblate shape. These structural characters observed in ^{187}Tl constitute good evidence for shape coexistence. The possible three-quasiparticle configurations and corresponding shapes at high excitation energy in ^{187}Tl are discussed.

ACKNOWLEDGMENTS

This work was supported by the National Key R&D Program of China under Grants No. 2022YFA1602302, No. 2018YFA0404403, and No. 2018YFA0404402, the National Natural Science Foundation of China under Grants No. U2167201, No. 12035001, No. 12075006, No. 11961141004, and No. 12135004, the Strategic Priority Research Program of Chinese Academy of Sciences (Grant No. XDB34010000). UK personnel are grateful for financial supportfrom the STFC, and A.N. Andreyev is partially funded by the Chinese Academy of Sciences President's International Fellowship Initiative (Grant No. 2020VMA0017). This work was also supported by the U.S. Department of Energy, Office of Nuclear Physics, under Contract No. DE-AC02-06CH11357 and Grants No. DE-FG02-94ER41041 (UNC) and DE-FG02-97ER41033 (TUNL), by the Slovak Research and Development Agency (Contract No. APVV-22-0282) and Slovak Grant Agency VEGA (Project 1/0651/21). This research used resources of ANL's ATLAS facility, which is a DOE Office of Science User Facility. The authors acknowledge the Target Labor team of GSI for preparing the targets for the experiment.

[1] K. Heyde and J. L. Wood, Rev. Mod. Phys. **83**, 1467 (2011).
[2] A. N. Andreyev, M. Huyse, P. Van Duppen, L. Weissman, D. Ackermann, J. Gerl, F. P. Hessberger, S. Hofmann, A. Kleinboehl, and G. Muenzenberg, Nature **405**, p.430.
[3] J. Wauters, P. Decrock, P. Dendooven, M. Huyse, G. Reusen, and P. Van Duppen, Z. Phys.A **339**, 533 (1991).
[4] P. Misaelides, P. Tidemand-Petersson, U. J. Schrewe, I. S. Grant, R. Kirchner, O. Klepper, I. C. Malcolm, P. J. Nolan, E. Roeckl, W. D. Schmidt-Ott, and J. L. Wood, Z. Phys.A **301**, 199 (1981).
[5] A. G. Schmidt, R. L. Mlekodaj, E. L. Robinson, F. T. Avignone, J. Lin, G. M. Gowdy, G. L. Wood, and R. W. Fink, Phys. Lett. B **66**, 133 (1977).
[6] A. P. Byrne, A. M. Baxter, G. D. Dracoulis, S. M. Mullins, T. Kibédi, T. R. McGoram, K. Helariutta, J. F. C. Cocks, P. Jones, R. Julin, S. Juutinen, H. Kankaanpää, H. Kettunen, P. Kuusiniemi, M. Leino, M. Muikku, P. Nieminen, P. Rahkila, and A. Savelius, Eur. Phys. J. A **7**, 41 (2000).
[7] W. Reviol, L. L. Riedinger, J.-Y. Zhang, C. R. Bingham, W. F. Mueller, B. E. Zimmerman, R. V. F. Janssens, M. P. Carpenter, I. Ahmad, I. G. Bearden, R. G. Henry, T. L. Khoo, T. Lauritsen, and Y. Liang, Phys. Rev. C **49**, R587 (1994).
[8] G. J. Lane, G. D. Dracoulis, A. P. Byrne, P. M. Walker, A. M. Baxter, J. A. Sheikh, and W. Nazarewicz, Nucl. Phys. A **586**, 316 (1995).
[9] S. K. Chamoli, P. Joshi, A. Kumar, R. Kumar, R. P. Singh, S. Muralithar, R. K. Bhowmik, and I. M. Govil, Phys. Rev. C **71**, 054324 (2005).
[10] A. B. F. Lee, G. J. Lane, G. D. Dracoulis, A. O. Macchiavelli, P. Fallon, R. M. Clark, F. R. Xu, and D. X. Dong, EPJ Web of Conferences **35** (2012).
[11] H. A. Schuessler, E. C. Benck, F. Buchinger, H. Iimura, Y. F. Li, C. Bingham, and H. K. Carter, Hyperfine Interactions **74**, 13 (1992).
[12] A. E. Barzakh, L. K. Batist, D. V. Fedorov, V. S. Ivanov, K. A. Mezilev, P. L. Molkanov, F. V. Moroz, S. Y. Orlov, V. N. Panteleev, and Y. M. Volkov, Phys. Rev. C **86**, 014311 (2012).
[13] A. E. Barzakh, L. K. Batist, D. V. Fedorov, V. S. Ivanov, K. A. Mezilev, P. L. Molkanov, F. V. Moroz, S. Y. Orlov, V. N. Panteleev, and Y. M. Volkov, Phys. Rev. C **88**, 024315 (2013).
[14] A. J. Mitchell, P. F. Bertone, B. DiGiovine, C. J. Lister, M. P. Carpenter, P. Chowdhury, J. A. Clark, N. D'Olympia, A. Y. Deo, F. G. Kondev, E. A. McCutchan, J. Rohrer, G. Savard, D. Seweryniak, and S. Zhu, Nucl. Instr. and Meth. A **763**, 232 (2014).
[15] W. Q. Zhang, A. N. Andreyev, Z. Liu, D. Seweryniak, H. Huang, Z. H. Li, J. G. Li, C. Y. Guo, D. T. Doherty, A. E. Barzakh, P. Van Duppen, J. G. Cubiss, B. Andel, S. Antalic, M. Block, A. Bronis, M. P. Carpenter, P. Copp, B. Ding, Z. Favier, F. Giacoppo, T. H. Huang, X. H. Yu, B. Kindler, F. G. Kondev, T. Lauritsen, G. S. Li, B. Lommel, H. Y. Lu, M. Al Monthery, P. Mošať, Y. F. Niu, C. Raison, W. Reviol, G. Savard, S. Stolze, G. L. Wilson, H. Y. Wu, Z. H. Wang, F. R. Xu, Q. B. Zeng, and X. H. Zhou, Phys. Lett. B **829**, 137129 (2022).
[16] H. Huang, W. Q. Zhang, A. N. Andreyev, Z. Liu, D. Seweryniak, Z. H. Li, C. Y. Guo, A. E. Barzakh, P. Van Duppen, B. Andel, S. Antalic, M. Block, A. Bronis, M. P. Carpenter, P. Copp, J. G. Cubiss, B. Ding, D. T. Doherty, Z. Favier, F. Giacoppo, T. H. Huang, B. Kindler, F. G. Kondev, T. Lauritsen, J. G. Li, G. S. Li, B. Lommel, H. Y. Lu, M. Al Monthery, P. Mošať, Y. F. Niu, C. Raison, W. Reviol, G. Savard, S. Stolze, G. Wilson, H. Wu, Z. Wang, F. Xu, Q. Zeng, X. Yu, F. Zeng, and X. Zhou, Phys. Lett. B **833**, 137345 (2022).
[17] W. Q. Zhang, A. N. Andreyev, Z. Liu, D. Seweryniak, H. Huang, Z. H. Li, J. G. Li, C. Y. Guo, A. E. Barzakh, P. Van Duppen, M. Al Monthery, B. Andel, S. Antalic, M. Block, A. Bronis, M. P. Carpenter, P. Copp, J. G. Cubiss, B. Ding, D. T. Doherty, Z. Favier, F. Giacoppo, T. H. Huang, B. Kindler, F. G. Kondev, T. Lauritsen,

G. S. Li, B. Lommel, H. Y. Lu, P. Mošať, Y. F. Niu, C. Raison, W. Reviol, G. Savard, S. Stolze, G. L. Wilson, H. Y. Wu, Z. H. Wang, F. R. Xu, X. H. Yu, Q. B. Zeng, and X. H. Zhou, Phys. Rev. C **106**, 024317 (2022).
[18] D. C. Radford, Nucl. Instr. and Meth. A **361**, 297 (1995).
[19] D. M. Cullen, N. Amzal, A. J. Boston, P. A. Butler, A. Keenan, E. S. Paul, H. C. Scraggs, A. M. Bruce, C. M. Parry, J. F. C. Cocks, K. Helariutta, P. M. Jones, R. Julin, S. Juutinen, H. Kankaanpää, H. Kettunen, P. Kuusiniemi, M. Leino, M. Muikku, and A. Savelius, Phys. Rev. C **58**, 846 (1998).
[20] J. Meng, J. Peng, S.-Q. Zhang, and P.-W. Zhao, Frontiers of Physics **8**, 55 (2013).
[21] R. Manvelyan, K. Mkrtchyan, W. Rühl, and M. Tovmasyan, Phys. Lett. B **699**, 187 (2011).
[22] P. W. Zhao, J. Peng, H. Z. Liang, P. Ring, and J. Meng, Phys. Rev. Lett. **107**, 122501 (2011).
[23] P. W. Zhao, Z. P. Li, J. M. Yao, and J. Meng, Phys. Rev. C **82**, 054319 (2010).